



“Gheorghe Asachi” Technical University of Iasi, Romania



EVALUATION OF MODIFIED FLY ASH BASED NAA-ZEOLITE: EFFECT OF CRYSTALLINITY ON CO₂ ADSORPTION CAPACITY

Muvumbu Jean-Luc Mukaba*, Alechine Emmanuel Ameh,
Chuks Paul Eze, Leslie Felicia Petrik

*Environmental and Nano Science Research Group, Department of chemistry, University of the Western Cape,
Robert Sobukwe Rd, Bellville, Cape Town, 7535, South Africa*

Abstract

NaA zeolite was successfully synthesised from fly ash through hydrothermal process. The synthesised NaA zeolite was modified with Li⁺, Ca²⁺ and Mg²⁺ through ion exchange at a temperature of 60 °C and contact times of 1 h and 4 h. In this study the crystallinity of the synthesised NaA as well as its modified (LiA, CaA and MgA) was evaluated towards CO₂ adsorption capacity using temperature programmed desorption (TPD) process at low temperature (40-150°C) and high temperature (150-700°C). The mineral phase and structural characteristics of zeolites were examined using XRD and FT-IR. The results from XRD and FT-IR spectra revealed unique structural alterations influenced by the intrinsic characteristic of individual cation incorporated in NaA zeolite. Monovalent cations displayed highest crystallinity compared to divalent cations (downward order: NaA > LiA > MgA > CaA). Low and high temperature CO₂-TPD profiles were independent of the degree of crystallinity of the zeolites and a significant amounts of CO₂ desorption occur at low temperature indicating that physisorption is the most prominent adsorption mode in NaA, LiA, CaA and MgA zeolite.

Key words: adsorption, carbon dioxide, crystallinity, ion exchange, synthesis, zeolite

Received: April, 2019; Revised final: August, 2019; Accepted: October, 2019; Published in final edited form: March, 2020

1. Introduction

Zeolites are crystalline aluminosilicates containing alkali, alkaline earth elements or other cations as charge balancing cations. Their structural framework is built up of three-dimensional networks containing (AlO₄)⁵⁻ and (SiO₄)⁴⁻ tetrahedra linked to each other by sharing of oxygen atoms (Querol et al., 2002). Their crystal structure contains pores and channels of molecular dimensions (Derkowski et al., 2007). Furthermore, the unique properties displayed by zeolites convey the usefulness of these materials in many applications as ion exchangers, molecular sieves, catalysts as well as the separation/adsorption of greenhouse gases such as carbon dioxide (CO₂) (Chalupnik et al., 2013; Walton et al., 2006). Zeolites

occurs naturally in igneous rocks (Fertu and Gavrilescu, 2012; Noor et al., 2019) or can be synthesized from materials with high silica (SiO₂) and alumina (Al₂O₃) content such as fly ash (FA) (Musyoka et al., 2012; Querol et al., 2002). The use of FA as a low-cost source of SiO₂ and Al₂O₃, in synthesis of zeolites such as NaA, is economically advantageous (Musyoka et al., 2012; Somerset et al., 2005). Various synthesis protocols for NaA from FA have been developed and discussed in the literature. The modifications or alternations in pretreatment steps in alkaline solutions is the fundamental step common in these protocols (Shaila et al., 2015).

For the past two decades, various studies have focused on the modifications of extra framework cation of NaA with alkali or alkaline earth metals such

* Author to whom all correspondence should be addressed: e-mail: 3258474@myuwc.ac.za, jeanlucmukaba@gmail.com; Phone: +27 219593878; Fax: +27 219593878

as calcium, magnesium, lithium etc., prior to CO₂ adsorption (Bae et al., 2013; Kyung-Mi and Young-Min, 2010). This modification is commonly carried out through ion exchange to compensate the charge of ions in the framework for electronic neutrality as well as to enhance the adsorption performances of NaA (Apreutesei et al., 2009; Rohling et al., 2018; Yang et al., 2010). In a study by Kyung-Mi and Young-Min, (2010) NaA and NaP1 were synthesised from FA by varying the NaOH/FA and NaAlO₂/FA ratios. The synthesized NaA and NaP1 were impregnated with Ca²⁺ and Mg²⁺ through an ion-exchange method prior to the adsorption of low-level CO₂ using Gas Chromatography technique. Their results showed that Ca²⁺ were best for the CO₂ adsorption owing to their electrostatic behavior and acid base interaction. In another approach, Bae et al., (2013), investigated the adsorption performances of NaA and NaX zeolites treated with alkaline metals (Ca²⁺ and Mg²⁺). The ion-exchanged zeolites sorbents obtained were tested for their potential application in post-combustion CO₂ capture at conditions relevant to a flue gas (0.15 bar and 40 °C) using high-throughput gas adsorption. Among the cation-exchanged zeolites assessed, CaA exhibited good performances for CO₂ adsorption/capture. This superior performance displayed by CaA arose from the strong binding of CO₂ within the 8-ring window of the framework and neighboring 6-rings of the extra-framework respectively as revealed by X-ray and neutron powder diffraction assessments. Whilst the aforementioned studies focused on converting NaA to CaA or MgA to enhance the performance of zeolites as well CO₂ adsorption capacity, only a few have discussed this performance with regard to the crystallinity (i.e quality of the crystal) of zeolite towards CO₂ adsorption capacity. This is because some characteristics of the zeolite crystal such as pore size and crystallinity alter depending upon the charge-balancing cation as well as cation size (Cheung et al., 2013). Rayalu et al. (2005) studied the structure development of FA based NaA during synthesis using XRD and FTIR.

The study revealed that the percent crystallinity calculated using standard procedure by XRD and FTIR were comparable; and that FTIR was the best option for estimating crystallinity and structure elucidation. Therefore, in this study, the XRD peaks and FTIR vibration bands intensities in tandem will be used in monitoring the crystallinity. The aim of this work is to synthesize NaA from FA and focuses on the evaluation of zeolite crystallinity as a function of the different cations exchanged (Li⁺, Na⁺, Ca²⁺ and Mg²⁺) towards CO₂ adsorption capacity at low or high temperatures. The quality of the cation exchanged zeolite crystals will be investigated with regard to their CO₂ physisorption or chemisorption efficiency.

2. Experimental

The synthesis conditions for NaA were revised and carried out as also described by Ameh et al.,

(2016). Prior to the synthesis, FA feedstock was mixed with sodium hydroxide (NaOH, 99 % purity) in the ratio of 1:1.2 respectively. This mixture was thoroughly ground for 5 min due to the hygroscopic behavior of NaOH. Thereafter, the resultant mixture was fused at a temperature of 550 °C for 1.5 h. The resulting fused sample was then crushed and mixed with deionized water prior to stirring in a solid: liquid (S:L) ratio of 2:10.

Afterwards, the slurry was set to agitate at room temperature for 2 h at 600 rpm and then filtered. 50 mL of the filtrate was added to 20 mL of NaAlO₂ (0.8 M) for hydrothermal synthesis in an unstirred pressure vessel at 100 °C in a hot air oven. The ion exchange was carried out using a S:L ratio of 1:10 of the synthesized NaA and aqueous (1 M) salt solutions (CaCl₂·2H₂O or MgCl₂·6H₂O or LiCl). This mixture was subjected to a series of ion exchanges at a temperature of 60 °C and contact time of 1 h or 4 h. After each ion-exchange procedure, the solid sample was gravimetrically collected through centrifugation and the ion-exchange procedure was repeated three times with a fresh salt solution. In each case at the end of the fourfold ion exchange process, the product was thoroughly and repeatedly washed with deionized water and dried at 80 °C in a hot air oven.

3. Characterization of zeolites

The structure of the synthesized and ion exchanged zeolites was examined by powder X-ray diffraction (XRD: PW3830 X-ray generator, PANalytical; Cu-Kα, λ = 1.54056, 40 kV) and Fourier transformed infrared (FT-IR: PerkinElmer UATR Two). The relative degree of crystallinity was calculated using standard procedures as reported by Rayalu et al. (2005). In this study, seven major intense peaks located at 2θ = 7.2°, 10.2°, 12.5°, 16.1°, 21.6°, 23.8°, and 30.1° were considered for XRD while the vibration bands at 550-470 cm⁻¹ were used for FT-IR. The scanning electron microscope (SEM: ZEISS AURIGA) was used for morphological analysis. The physisorption and chemisorption process of zeolites was carried out using CO₂-TPD (AutoChem II 2920, Micromeritics).

Prior to CO₂-TPD analysis, zeolite (100 mg) was degassed in helium at 300 °C (ramping rate 10 °C/min and helium flow rate 20 mL/min). CO₂-TPD adsorption experiments were commenced at a holding temperature of 40 °C in helium at flow rate of 20 mL/min and 10 mL/min for helium and CO₂ respectively. Instrument grade CO₂ (99.999 %) was allowed to pass over the sample for 2 h (saturation time).

Following the CO₂ saturation and flush out of excess CO₂ with helium, the thermal conductivity detector (TCD) was turned on; it was allowed to stabilize and then zeroed. The sample was heated at 5 °C/min within two regions of desorption temperatures at 40-150 °C (low temperature desorption peaks) and from 150-700 °C (high temperature desorption peaks). The amounts of CO₂ desorbed from zeolites

adsorption sites were evaluated using the Peak Fit v4.12 integrations of TCD signals.

4. Results and discussions

4.1. Characterization

Fig. 1 shows the XRD patterns of FA, fused fly ash (FFA) and the synthesized NaA zeolite. The XRD results revealed that the FA used for the synthesis contained a small amount of hematite (H) whereas mullite (M) and quartz (Q) were the main phases. The presence of mullite, and quartz mineral phases have been also reported in the literature (Ge et al., 2018; Rayalu et al., 2005). These phases are believed to act as resistant aluminosilicates phases and can hinder the conversion of FA to the zeolitic phase (Kyung-Mi and Young-Min, 2010). The fusion step is crucial prior to the synthesis since mineral phases such as mullite and quartz originated from FA can potentially remain in the synthesized zeolite (Ryu et al., 2006).

The XRD results showed that both mullite and quartz phases completely decomposed during the thermal alkaline fusion and the main mineral phases observed in FFA were sodium-aluminate (SA) and sodium silicate (SS). The SA and SS mineral phases in turn hydrothermally converted to crystalline

zeolite-A phase, which typical peaks appeared in FA based zeolite-A product referred to as synthesized NaA zeolite in this study. The XRD also showed that no FA or FFA mineral phases remained in the zeolite product. This was an indication of the successful formation of a pure phase of NaA zeolite.

The SEM micrographs of FA, FFA and NaA revealed that, the FA as received (Fig. 2a) were spherically shaped with smooth surfaces compared to the agglomerated FFA (Fig. 2b). Ge et al., (2018), Harja et al., (2008) also discussed these morphological characteristics of FA. However, the morphological changes observed in FFA are as a result of alkaline dissolution of FA as produced through fusion (Bukhari et al., 2014; Musyoka et al., 2011). The alkaline dissolution of FA resulted in a new mineral phase observed in FFA (Fig. 1).

Furthermore, the hydrothermal synthesis process using the FFA filtrate added to the sodium aluminate solution resulted in crystalline, chamfered cubic particles which ranged between 1-2 μm in size (Fig. 3). These chamfered cubic crystals corresponded to the typical NaA zeolite morphology (Fig. 2c). The characteristics of NaA zeolite synthesized in this work have also been reported by Kyung-Mi and Young-Min, (2010); Musyoka et al., (2012).

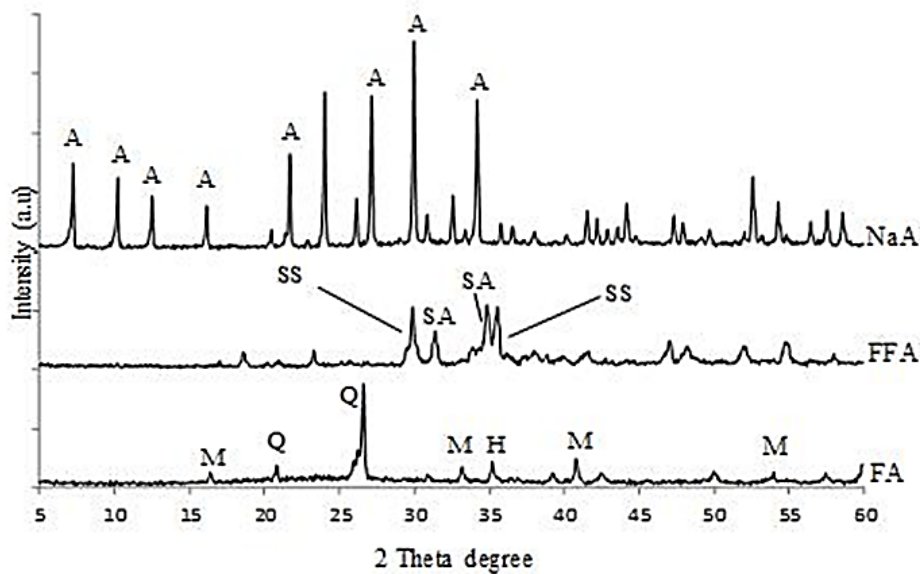


Fig. 1. XRD patterns of the synthesised fly ash based NaA zeolite, fused fly ash (FFA) and untreated fly ash (FA)

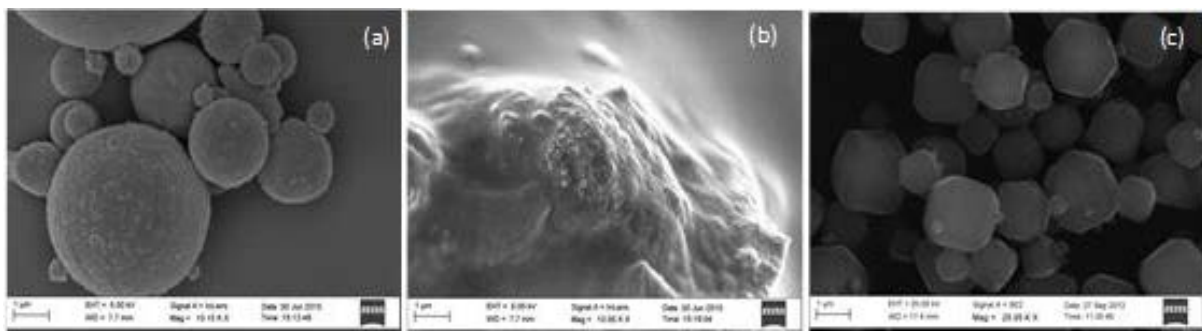


Fig. 2. SEM images of untreated fly ash (a) fused fly ash (b) and synthesised fly ash based NaA zeolite (c)

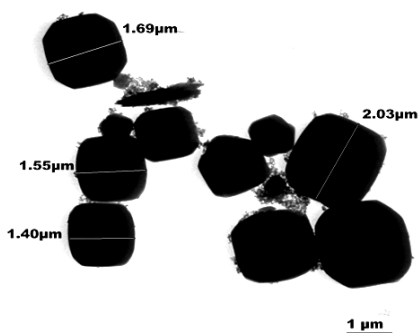


Fig. 3. Particles size of the synthesised NaA zeolite

4.2. Ion exchange

The XRD patterns of the synthesized NaA and its exchanged forms (LiA, CaA and MgA) at contact time of 1 h and 4 h are shown in Fig. 4. The exchanged zeolites revealed a typical structural framework that was similar to NaA zeolite. Although the frameworks were fairly retained; a relatively variation in peak intensities and peak shifting between 2θ : 20° and 60° were observed in all the XRD patterns of exchanged zeolites. Peak intensities and shifting were found correlating with the inherent characteristics of each cation rather than the contact time or temperature of exchange. LiA displayed the highest peak intensities compared to CaA and MgA zeolites. This effect might be caused by the small radius of the charge compensating Li^+ cation associated with Al^{3+} which is

part of the lattice framework. Furthermore, the Li atom is nearly three times smaller than the Na atom though both atoms provide similar charge compensation via their monovalent charge.

The substitution of Na atoms by Li atoms for charge compensation in NaA zeolite might have decreased the interatomic distances (d-spacing) (Table 1) causing higher peak intensities and peaks shifting to higher 2θ values. Unlike the XRD patterns of LiA ; CaA and MgA zeolites revealed ascending peaks. These peaks were mainly located between 2θ values $5-20^\circ$. New peaks arising and collapsing such as the peak at 2θ values 20.46° in CaA might confirm the structural changes that occurred in the crystal lattice of the parent zeolite due to high atomic radius of Ca^{2+} (99 pm) cation relative to Mg^{2+} (65 pm) and Li^+ (60 pm) cations. This behavior of Ca^{2+} cation could be in good agreement with Luhrs et al., (2012).

The XRD peaks that arose at 2θ values 14.5° and 17.6° are both attributed to zeolite-A phases according to Treacy and Higgins (2001). However, these two peaks only appeared with divalent cations (Ca^{2+} and Mg^{2+}). These peaks might have been due to the interactions between the divalent charge compensation and the positioning of both Ca^{2+} and Mg^{2+} cations in the framework of zeolite-A (Bae et al., 2013). XRD patterns of Mg based zeolites also showed a typical decrease in peak intensities at 2θ values 10.2° and 16.1° . This decrease may be due to the high electronegativity of the Mg^{2+} cation in comparison to Li^+ and Ca^{2+} cations.

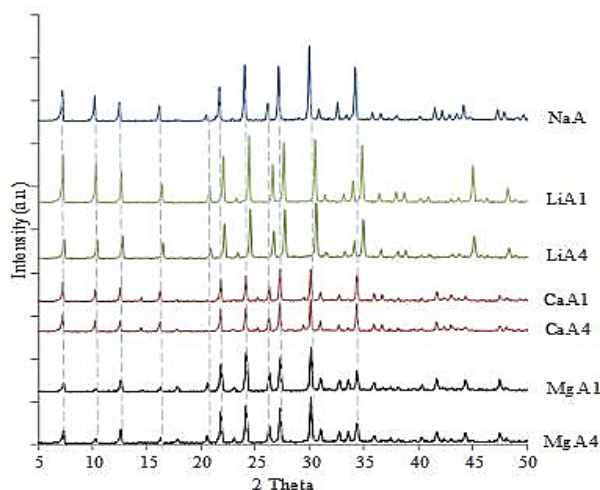


Fig. 4. XRD patterns of the synthesized NaA and zeolites exchanged at 1 h (LiA1, CaA1, MgA1); 4 h (LiA4, CaA4, MgA4).

Table 1. d-spacing values of synthesized (*) and exchanged zeolites

h k l	2θ	d space						
		NaA*	LiA1	LiA4	CaA1	CaA4	MgA1	MgA4
2 0 0	7.18	12.333	12.062	12.042	12.268	12.254	12.306	12.281
2 2 0	10.17	8.714	8.520	8.093	8.670	8.658	8.711	8.664
2 2 2	12.46	7.104	6.956	6.922	7.073	7.048	7.091	7.072
4 2 0	16.11	5.499	5.386	5.365	5.478	5.463	5.479	5.474
6 0 0	21.67	4.099	4.015	4.011	4.083	4.079	4.094	4.083
6 2 2	23.99	3.708	3.811	3.808	3.703	3.689	3.702	3.668
8 2 2	30.83	2.898	2.922	2.913	2.872	2.869	2.891	2.889

Amongst other cations incorporated in zeolite NaA, Ca²⁺ showed drastically loss of peaks intensities while Li⁺ displayed the highest intensities (Fig. 4). The descending order in terms of peak intensities was as follows: NaA > LiA > MgA > CaA for both short and extended ion exchange. The lower peak intensities observed in CaA and MgA zeolites is essentially attributed to their respective high electron density relative to the inherent zeolitic atoms of the framework (Al, Si and O) and the compensating Na atom. These low peak intensities observed in CaA and MgA zeolites were in good agreement with the results of Bronic et al. (2006); Lee et al. (2012).

Fig. 5 shows the FT-IR spectra of NaA, LiA, CaA and MgA zeolites. The vibration bands at 462 cm⁻¹ and 546 cm⁻¹ are characteristic of T-O double ring internal and T-O double ring external linkages respectively (Deng et al., 2016; Hashemian et al., 2013; Watanabe et al., 2004). The ratio of the intensities of these two absorption bands is indicative of the degree of the crystallinity of zeolitic material (Rayalu et al., 2005; Shirazi et al., 2008). In this study, the ratios of bands at 462 cm⁻¹ and 546 cm⁻¹ (Table 2) of zeolites were between 0.81-1.83. These values compared to the literature value of 1.85 for NaA zeolite, showed that the as-synthesized NaA zeolite with the highest value of 1.83 exhibited good crystallinity confirming high intensity peaks observed in the XRD patterns.

CaA zeolites tended to display weak band intensities at 462 cm⁻¹ and 546 cm⁻¹ in comparison to LiA and MgA zeolites. This might confirm the low peak intensities observed in the XRD patterns of CaA zeolites. The high decreased intensity observed at 462 cm⁻¹ in both CaA and MgA zeolites may be due to high charge density compensation. This result is in good agreement with Mozgawa et al. (2009). Ca²⁺ and Mg²⁺ being divalent cations tended to display lower intensity vibrational bands compared to the monovalent Na⁺ and Li⁺ cations which showed higher intensity bands at this position.

The structural changes observed at the vibration bands at 665 cm⁻¹ and 970 cm⁻¹ were essentially related to the inherent characteristic of each cation. The vibration at 665 cm⁻¹ is attributed to symmetric stretching and may be related to Al-O-M interactions according to Kugbe et al. (2009) (M=extra-framework cation). The intensity of this

vibration varies inversely with the atomic size of each cation. Thus, LiA zeolites displayed an intense vibration at this position compared to CaA and MgA zeolites. The Li⁺ (60 pm) cation is smaller than the Na⁺ (95 pm) cation (host cation), though both cations are monovalent.

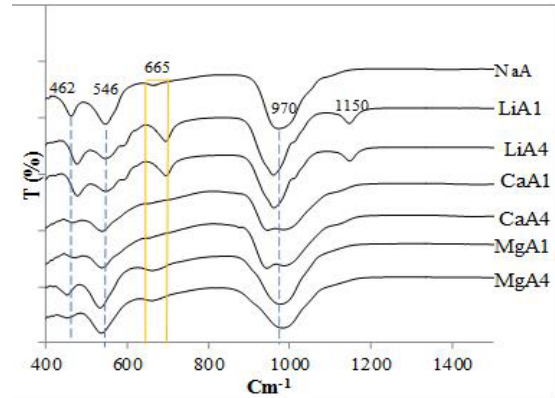


Fig. 5. FT-IR spectra of the synthesised NaA and zeolites exchanged at 1 h (LiA1, CaA1, MgA1); 4 h (LiA4, CaA4, MgA4)

The band at 970 cm⁻¹ is attributed to the asymmetric stretching of T-O-T (T=Si or Al). This band depicted distinctive shapes for each cation. CaA zeolites were displaying a doublet band instead of a narrowed shape initially observed in the parent synthesized NaA zeolite and other zeolites. This doublet band observed with Ca²⁺ might be characteristic of CaA zeolites as also reported by De Pena and Rondon (2013). This behavior from Ca²⁺ discerned by FT-IR might be due to high atomic size relatively to Li⁺ and Mg²⁺ and also the interactions between Ca²⁺ cation and the structural framework of zeolite A. However, the band appearing at 1150 cm⁻¹ in Li exchanged zeolites was assigned to asymmetric stretching of the O-T-O which might resulted from the interaction between the Li⁺ cation and the framework of zeolite.

4.3 Adsorption

The CO₂-TPD profiles of NaA and its exchanged forms (LiA, CaA and MgA) obtained respectively at low and high temperature are given in Figs. (6-7).

Table 2. Relative degree of crystallinity from FT-IR and XRD

Zeolites	FT-IR peak intensities (A)		Ratio (a/b)	Crystallinity (%)	
	546 cm ⁻¹ (a)	462 cm ⁻¹ (b)		FT-IR	XRD
NaA	0.53	0.29	1.83	100	100
LiA1	1.35	0.97	1.39	76.1	91.3
LiA4	1.55	1.12	1.38	75.7	79.2
CaA1	1.1	1.14	0.96	52.7	53.4
CaA4	0.75	0.83	0.91	49.4	42.5
MgA1	0.81	0.66	1.22	67.1	62
MgA4	1.21	1.09	1.11	60.7	50.5

Although the effect of contact time was not well discerned through the XRD and FTIR, the TPD profiles however revealed a significant increase of CO₂ adsorption in particular at low temperature for zeolites exchanged at the extended time (Fig. 6 b).

The unique desorption peaks observed between 60 and 100 °C at low temperature were ascribed to CO₂ desorbed from weak acid sites referred to as physisorption process. Physisorption was found as the main adsorption mode in which CO₂ desorption occurred for the aforementioned zeolites-A. This adsorption trend was also reported by Cheung et al. (2013), while investigating the adsorption of CO₂ in different crystal sizes zeolite-NaA. CO₂ desorbed from weak sites was surprisingly high in FA based NaA compared to the modified zeolites. This indicates that some of the acid sites initially present on the unmodified NaA might have been altered during the ion exchange.

Amongst the modified zeolites, CO₂ physisorbed prevailed in CaAs followed by MgAs and LiAs for both 1h and 4 h. Their CO₂ adsorption capacities were proportional to increased contact time and correlated to the removal of the host Na⁺ as could be seen in Fig. 8. Also, Fig. 8, revealed that the highest Na⁺ removal was found with Ca²⁺ followed by Mg²⁺ and Li⁺ respectively and might be as a result of its high ionic size relatively to Li and Mg and the host Na cation as discussed in section 4.2.

Whilst, low temperature CO₂ desorption profiles were predominately controlled by physisorption, high temperature displayed poor desorption in which peak fitting technique was employed to evaluate CO₂ behavior. The peak fitting revealed that, the monovalent based zeolites (i.e NaA and LiA) depicted low CO₂ capacities compared to divalent zeolites CaA and MgA.

This may result from strong interactions that exist between divalent cations (Ca²⁺ and Mg²⁺) and CO₂ molecules as compared to monovalent cations (Li⁺ and Na⁺). These interactions at high temperature (450-600 °C) as well the distinctive CO₂ desorption profiles might seemingly be due to the formation of carbonates. Carbonates formation in NaA at high temperature has been reported by Bae et al., (2013). As it can be seen from Fig.9, the highest crystallinities were found in LiAs followed by MgAs and CaAs (NaA > LiA > MgA > CaA).

Both XRD and FTIR showed a similar trend and were complementary in the evaluation of the crystallinity as reported by Rayalu et al., (2005). Furthermore, this crystallinity seemingly varies with the exchange of the host Na⁺ as high removal tended to generate LiAs, CaAs or MgAs with low crystallinities and was inversely proportional to CO₂ adsorption capacities. However, despite their relatively high crystallinities discerned from the XRD and FTIR, the LiA and MgA zeolites did not induce improved CO₂ capacity performances compared to CaA notwithstanding a lower crystallinity that was observed in particular for zeolites exchanged at 4 h. This undoubtedly indicates that inherent characteristic of individual cation is the main driving force controlling the CO₂ adsorption capacity.

5. Conclusions

The formation of a chamfered cubic crystal and XRD phase identification indicate the direct conversion of South African FA into typical zeolite-A morphology. The variation in XRD and FTIR peak intensities of the modified zeolites is a function of the individual intrinsic characteristic of Li⁺, Ca²⁺ and Mg²⁺ cation.

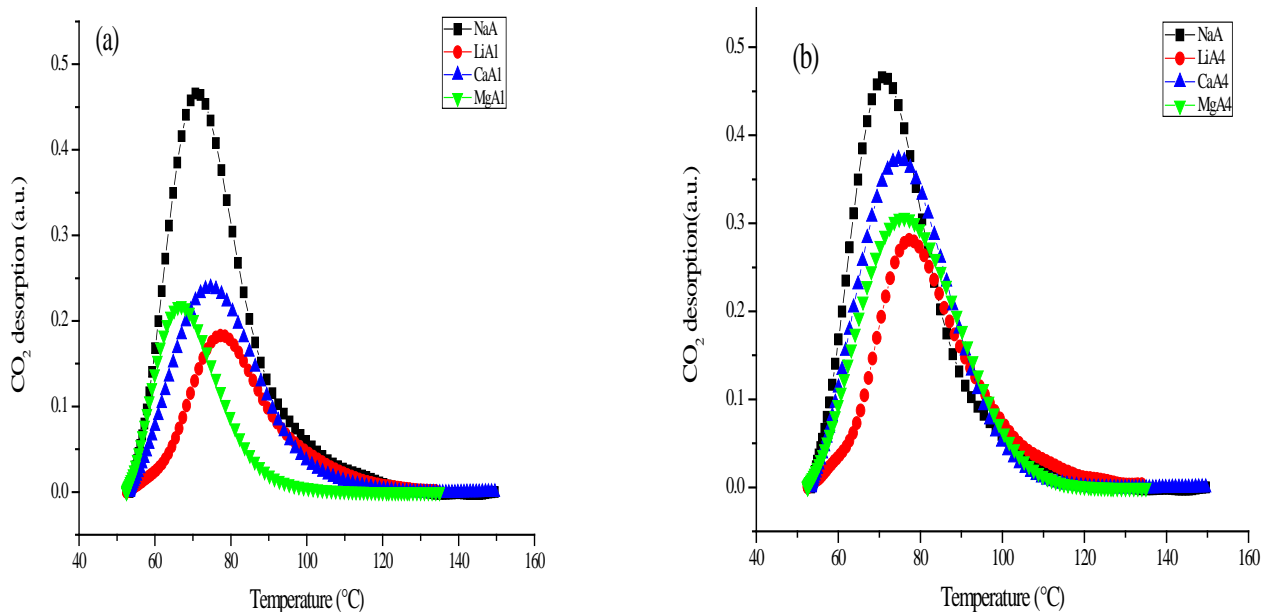


Fig. 6. CO₂-TPD profiles at low temperature (40-150 °C) of the synthesized NaA and zeolites exchanged at 1 h (a); 4 h (b).

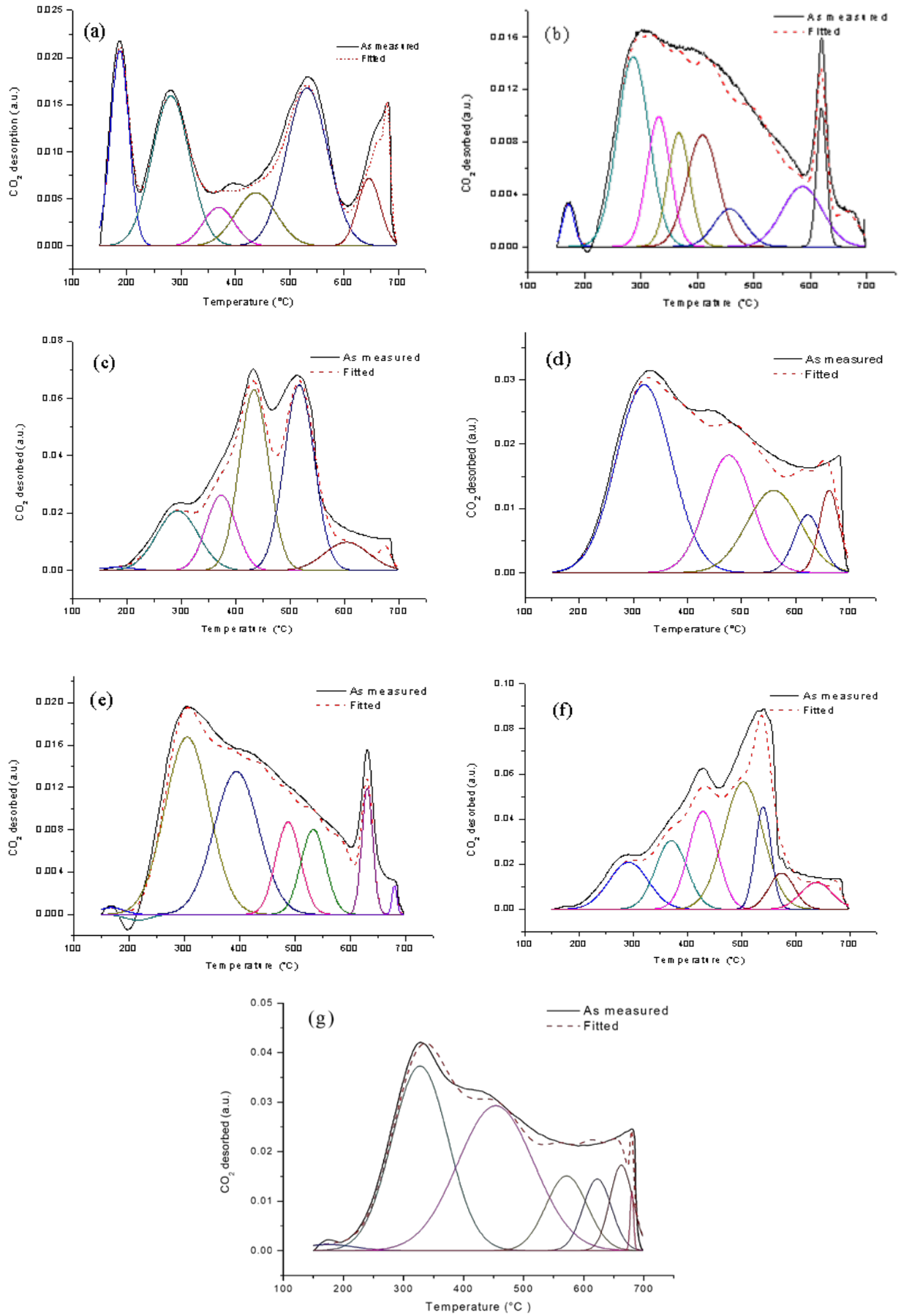


Fig. 7. CO₂-TPD profiles at high temperature (150-700 °C) of (a) NaA and exchanged zeolites at 1 h: (b) LiA1, (c) CaA1 (d) MgA1 and 4 h: (e) LiA4 (f) CaA4, (g) MgA4

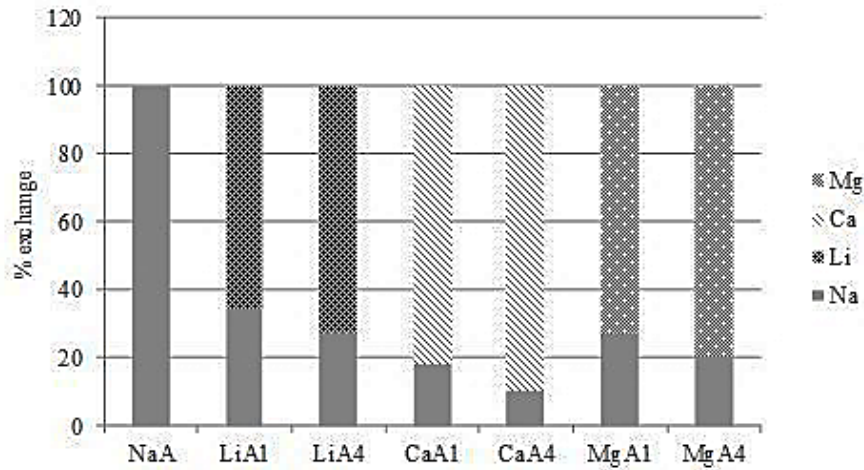


Fig. 8. Loading capacity behavior of Li, Ca and Mg cations in the synthesised NaA zeolite at 1 h and 4 h.

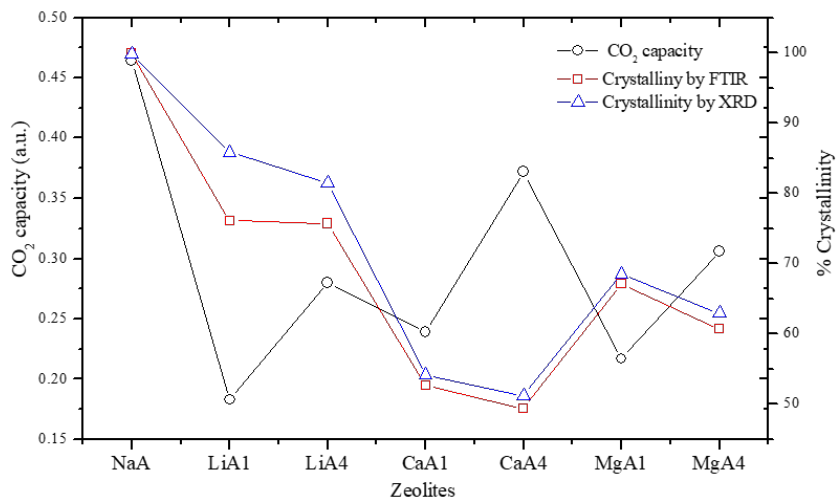


Fig.9. CO₂ adsorption capacities and the crystallinity of zeolites

The XRD and FTIR peak intensities as indicative of the degree of crystallinities of the zeolites were as follows in the descending order: NaA > LiA > MgA > CaA. CO₂ adsorption at low and high temperature is independent of the degree of the crystallinity of NaA, LiA, CaA and MgA and essentially occurs though physisorption process as the main interaction.

This study has proved that the quality of the zeolite crystal referred to as crystallinity in this study has no effects on its CO₂ adsorption capacity rather the inherent properties of individual cation is the main driving force during the adsorption process. This study is to foresee the utilization of the low quality FA based zeolite-A in CO₂ sequestration.

References

- Ameh A.E., Musyoka N.M., Fatoba O.O., Syrtsova D.A., Teplyakov V.V., Petrik, L.F., (2016), Synthesis of zeolite NaA membrane from fused fly ash extract, *Journal of Environmental Science and Health, Part A*, **51**, 348-356.
- Apreutesei R.E., Catrinescu C., Ungureanu A., Teodosiu C., (2009), Removal of 4-chlorophenol by surfactant modified zeolites and surfactant modified alkali-treated natural zeolites, *Environmental Engineering and Management Journal*, **8**, 1053-1060.
- Bae T.H., Hudson M.R., Mason J.A., Queen W.L., Dutton J.J., Sumida K., Long J.R., (2013), Evaluation of cation-exchanged zeolite adsorbents for post-combustion carbon dioxide capture, *Energy and Environmental Science*, **6**, 128-138.
- Bronic J., Sekovanic L., Muzic A., Biljan T., Kontrec J., Subotic B., (2006), Host-guest interaction of iodine with zeolite A, *Acta Chimica Slovenica*, **53**, 166-171.
- Bukhari S.S., Behin J., Kazemian H., Rohani S., (2014), A comparative study using direct hydrothermal and indirect fusion methods to produce zeolites from coal fly ash utilizing single-mode microwave energy, *Journal of Materials Science*, **49**, 8261-8271.
- Cheung O., Bacsik Z., Liu Q., Mace A., Hedin N., (2013), Adsorption kinetics for CO₂ on highly selective zeolites NaKA and nano-NaKA, *Applied Energy*, **112**, 1326-1336.
- Chalupnik S., Franus W., Wysocka M., Gzyl G., (2013), Application of zeolites for radium removal from mine water, *Environmental Science Pollution Research*, **20**, 7900-7906.

- Derkowski A., Franus W., Waniak-Nowicka H., Czi'merova' A., (2007), Textural properties vs. CEC and EGME retention of Na-X zeolite prepared from fly ash at room temperature, *International Journal Mineral Process*, **82**, 57-68.
- Deng L., Xu Q., Wu H., (2016), Synthesis of zeolite-like material by hydrothermal and fusion methods using municipal solid waste fly ash, *Procedia Environmental Sciences*, **31**, 662-667.
- De Pena Y.P., Rondon W., (2013), Linde type a zeolite and type Y faujasite as a solid-phase for lead, cadmium, nickel and cobalt preconcentration and determination using a flow injection system coupled to flame atomic absorption spectrometry, *American Journal of Analytical Chemistry*, **4**, 387-397.
- Fertu D.I.T., Gavrilescu M., (2012), Application of natural zeolites as sorbents in the clean-up of aqueous streams. *Environmental Engineering and Management Journal*, **11**, 867-878.
- Ge J., Yoon S., Choi N., (2018), Application of fly ash as an adsorbent for removal of air and water pollutants, *Applied Sciences*, **8**, 1116.
- Harja M., Bărbuță M., Rusu L., Apostolescu N., (2008), Utilization of coal fly ash from power plants I. Ash characterization, *Environmental Engineering and Management Journal*, **7**, 289-293.
- Hashemian S., Seyed H.H., Salehifar H., Salari K., (2013), Adsorption of Fe (III) from Aqueous Solution by Linde Type-A Zeolite, *American Journal of Analytical Chemistry*, **4**, 123-126.
- Kugbe J., Matsue N., Henmi T., (2009), Synthesis of Linde Type A Zeolite-Goethite Nanocomposite as an Adsorbent for Cationic and Anionic Pollutants, *Journal of Hazardous Materials*, **164**, 929-935.
- Kyung-Mi L., Young-Min J., (2010), Synthesis of Zeolite from waste fly ash for adsorption of CO₂, *Journal of Material Cycles Waste Management*, **12**, 212-219.
- Luhrs H., Jewgenij D., Reinhard X.F., (2012), K⁺ and Ca²⁺ exchange behavior of zeolite A, *Microporous and Mesoporous Materials*, **151**, 457-465
- Lee K.M., Lim Y.H., Park C.J., Jo Y.M., (2012), Adsorption of low-level CO₂ using modified zeolites and activated carbon, *Industrial & Engineering Chemistry Research*, **51**, 1355-1363.
- Mozgawa W., Król M., Bajda T., (2009), Application of IR spectra in the studies of heavy metal cations immobilization on natural sorbents, *Journal of Molecular Structure*, **924**, 427-433.
- Musyoka N.M., Petrik L., Hums E., (2011), Ultrasonic assisted synthesis of zeolite A from coal fly ash using mine waters (acid mine drainage and circumneutral mine water) as a substitute for ultra-pure water, *Proceedings of International Mineral Water Association, Aachen, Germany*, 423-428.
- Musyoka N.M., Petrik L., Hums E., (2012), Synthesis of zeolite A, X and P from a South African coal fly ash, *Advanced Materials Research*, **512**, 1757-1762.
- Noor A., Juzsakova T., Halmagyi T., Cretescu I., Sebestyen V., Balazs Z., Domokos E., Fazakas J., Redey A., (2019), Study on dealuminated zeolitic tuff for hydrocarbon removal from water, *Environmental Engineering and Management Journal*, **18**, 1809-1820.
- Querol X., Moreno N., Umaña J.C., Alastuey A., Hernández E., López-Soler A., Plana F., (2002), Synthesis of zeolites from coal fly ash: An overview, *International Journal of Coal Geology*, **50**, 413-423.
- Rayalu S.S., Udhoji J.S., Meshram, S.U., Naidu, R.R. and Devotta, S., (2005), Estimation of crystallinity in fly ash-based zeolite-A using XRD and IR spectroscopy, *Current Science*, 2147-2151.
- Rohling R.Y., Hensen E.J., Pidko E.A., (2018), Multi-site cooperativity in alkali-metal-exchanged faujasites for the production of biomass-derived aromatics, *ChemPhysChem*, **19**, 446-458.
- Ryu T.G., Ryu J.C., Choi C.H., Kim C.G., Yoo S.J., Yang H.S., Kim Y.H., (2006), Preparation of Na-P1 zeolite with high cation exchange capacity from coal fly ash, *Journal Industrial Engineering Chemistry*, **12**, 401-407.
- Shailla K., Nisha D., Pralhad P., Deepa P., (2015), Zeolite synthesis strategies from coal fly ash: a comprehensive review of literature, *International Research Journal in Environment Sciences*, **4**, 93-99.
- Shirazi L., Jamshidi E., Ghasemi M.R., (2008), The effect of Si/Al ratio of ZSM-5 zeolite on its morphology, acidity and crystal size, *Crystal Research and Technology*, **43**, 1300-1306.
- Somerset V.S., Petrik L.F., White R.A., Klink M.J., Key D, Iwuoha E.I., (2005), Alkaline hydrothermal zeolites synthesized from high SiO₂ and Al₂O₃ co-disposal fly ash filtrates, *Fuel*, **18**, 2324-2329.
- Treacy M.J., Higgins J.B., (2001), *Collection of Simulated XRD Powder Patterns for Zeolites*, 4th Edition. Elsevier, *Amsterdam*, **379**, 327-802.
- Walton K.S., Abney M.B., Douglas L.M., (2006), CO₂ adsorption in Y and X zeolites modified by alkali metal cation exchange, *Microporous Mesoporous Materials*, **91**, 78-84.
- Watanabe Y., Moriyoshi Y., Suetsugu Y., Ikoma T., Kasama T., Hashimoto T., Yamada H., Tanaka J., (2004), Hydrothermal formation of hydroxyapatite layers on the surface of type-A zeolite, *Journal of the American Ceramic Society*, **87**, 1395-1397.
- Yang S.T., Kim J., Ahn W.S., (2010), CO₂ adsorption over ion-exchanged zeolite beta with alkali and alkaline earth metal ions, *Microporous and Mesoporous Materials*, **135**, 90-94.